

Spin-Wave Optical Elements: Towards Spin-Wave Fourier Optics

M. Vogel,^{1, a)} B. Hillebrands,¹ and G. von Freymann^{1, 2}¹⁾Department of Physics and State Research Center OPTIMAS, Technische Universität Kaiserslautern (TUK), Erwin-Schrödinger-Str. 56, 67663 Kaiserslautern, Germany²⁾Fraunhofer-Institute for Industrial Mathematics ITWM, Fraunhofer-Platz 1, 67663 Kaiserslautern, Germany

(Dated: 7 June 2019)

We perform micromagnetic simulations to investigate the propagation of spin-wave beams through spin-wave optical elements. Despite spin-wave propagation in magnetic media being strongly anisotropic, we use axicons to excite spin-wave Bessel-Gaussian beams and gradient-index lenses to focus spin waves in analogy to conventional optics with light in isotropic media. Moreover, we demonstrate spin-wave Fourier optics using gradient-index lenses. These results contribute to the growing field of spin-wave optics.

Spin waves are eigenmodes of a magnetic solid body – magnons are their quasiparticles. Spin-wave dispersion relations and the corresponding magnonic refractive indices depend not only on the orientation of the external magnetic field but also on several other parameters. Hence, spin-wave propagation is very complex and strongly anisotropic in contrast to light in isotropic media. Recently, spin-wave optics gains increasing attention as it can be seen as a prerequisite for spin-wave based data-processing. In 2016, Gruszecki *et al.* showed theoretically how to excite Gaussian spin-wave beams using narrowed microwave antennas¹. In the same year, Snell's law of refraction has been verified experimentally in a magnonic system². Also in 2016, the concept of spin-wave fibers to guide magnons using the Dzyaloshinskii-Moriya interaction has been shown theoretically by Xing *et al.*³ and Yu *et al.*⁴ independently. Moreover, different concepts to focus spin waves using the modulation of the film thickness⁵ or heating via a laser spot⁶ have been introduced. Further spin-wave optical elements have been developed in the following year such as Fresnel⁷ and Luneburg lenses⁸. The concept of spin-wave beam excitation via narrowed antennas has been demonstrated experimentally by Körner *et al.* in the same year⁹. In addition to the described concepts, gradients of the magnetic field and the saturation magnetization have the potential to guide spin waves in magnetic media^{10–13}. Moreover, magnonic crystals^{14–16} have the potential to control and manipulate spin-wave propagation via tailored dispersion relations as well.

In this Letter we demonstrate that the powerful concept of Fourier optics not only holds for out-of-plane magnetized magnetic films with an in-plane isotropic spin-wave dispersion relation but also for in-plane magnetization and its corresponding anisotropic spin-wave dispersion. In order to obtain a deeper insight we perform micromagnetic simulations. Using the open-source software MuMax3, which solves the Landau-Lifshitz-Gilbert equation¹⁷

$$\frac{d}{dt} \vec{m}(\vec{r}, t) = \frac{\gamma}{1 + \alpha^2} \left\{ \vec{m}(\vec{r}, t) \times \vec{B}_{\text{eff}}(\vec{r}, t) + \alpha \left[\vec{m}(\vec{r}, t) \times \left(\vec{m}(\vec{r}, t) \times \vec{B}_{\text{eff}}(\vec{r}, t) \right) \right] \right\} \quad (1)$$

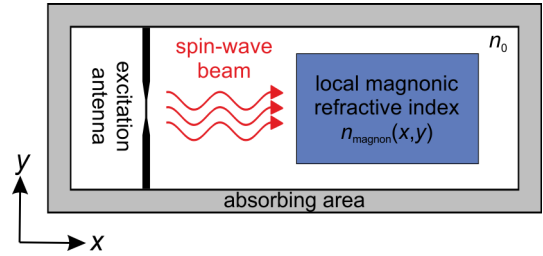
^{a)}Electronic mail: mvogel@physik.uni-kl.de

FIG. 1. Scheme of the simulation area to excite spin-wave Gaussian beams and to study the propagation behavior in landscapes of the magnonic refractive index.

on a rectangular grid, we study spin-wave propagation in landscapes of the magnonic refractive index. Here, $\vec{m} = \vec{M}/M_S$ is the normalized vector of the magnetization \vec{M} with respect to the saturation magnetization M_S . The effective magnetic field \vec{B}_{eff} includes the demagnetizing and exchange field, Ruderman-Kittel-Kasuya-Yoshida interaction, cubic and uniaxial anisotropy, thermal fluctuations, and the Dzyaloshinskii-Moriya interaction. γ is the gyromagnetic ratio and α describes the Gilbert damping parameter. To achieve spin-wave propagation over large distances, the sample system of choice for the simulation of spin-wave optics is a 5 μm thick yttrium iron garnet (YIG) film. YIG has the smallest known damping parameter¹⁶ (here $\alpha = 10^{-4}$). Depending on the relative orientation of the external magnetic field with respect to the surface of the YIG film and the propagation direction, different spin-wave modes exist. If the external field is oriented out-of-plane, forward volume magnetostatic spin waves (FVMSWs) exist. Due to symmetry reasons no in-plane propagation direction is favored¹⁸. Hence, the isofrequency curves are circles in analogy to the dispersion relation of light in conventional optics. In contrast, spin-wave propagation in in-plane magnetized samples is non-trivial: For spin-wave propagation parallel to the external field direction the modes are called backward volume magnetostatic spin waves (BVMSWs). In perpendicular direction to the external field magnetostatic surface spin waves (MSSWs) propagate. The resulting anisotropic isofrequency curves of BVMSW and MSSW modes are more complex. In first approximation, they are parabolic with orthogonal symmetry axis (see Refs. 19 and 20).

The scheme of our calculations is shown in Figure 1. The

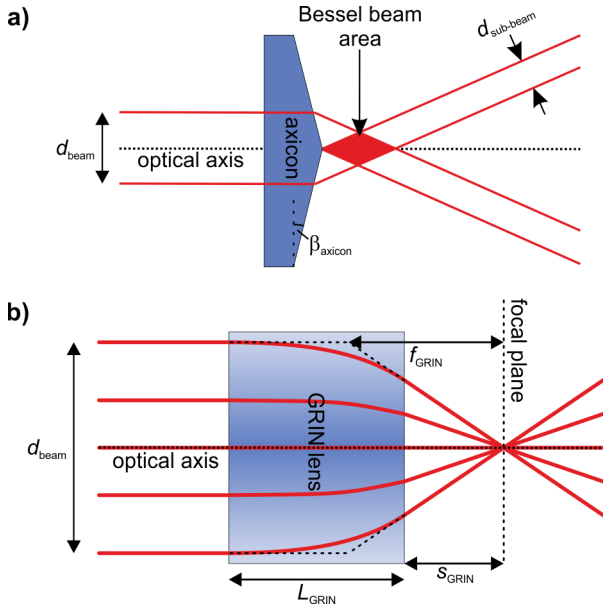


FIG. 2. Scheme of two landscapes of the magnonic refractive index: (a) a spin-wave axicon is formed by a triangular shaped region with constant temperature, while (b) a GRIN lens contains a temperature gradient in a rectangular area.

Oersted field of a narrowed microstrip antenna excites spin-wave Gaussian beams. To reduce undesired reflections at the edges of the simulation area we implement a 1 mm wide absorbing boundary in which the damping parameter increases exponentially to $\alpha = 1$. The blue marked region contains the magnonic refractive index profile that modifies the propagation of the spin-wave beam. We approximate the magnonic refractive index in analogy to optics as follows:

$$n_{\text{magnon}} = \frac{ck}{\omega(k)}. \quad (2)$$

Here, c is the speed of light in vacuum, k the spin-wave wavenumber, and $\omega(k)$ the dispersion relation obtained by solving the Landau-Lifshitz-Gilbert equation (1). The dispersion relation of the respective spin-wave mode depends on many different parameters^{12,13,21–25}. Here, we change the local temperature T and therefore the saturation magnetization $M_S(T)$ ¹⁵: $M_S \propto -T$. It is assumed, that the sample is heated homogeneously across the film thickness. In this case n_{magnon} does not depend on the z coordinate and in the simulation only one cell unit is used for this coordinate. In the following, spin-wave propagation through landscapes of the magnonic refractive index equivalent to axicons and gradient-index (GRIN) lenses (see Figure 2) is investigated.

I. SPIN-WAVE AXICONS

Besides the excitation of Gaussian beams, other beams with a more complex profile can be created such as a Bessel-Gaussian beam²⁶ which is used in photonics e.g. as optical tweezer²⁷. To realize such a beam in optics, a conical

TABLE I. Parameter of the Bessel-Gaussian beam.

parameter	fitted value
A	0.995 ± 0.008
B	0.011 ± 0.002
y_0	$(7.500 \pm 0.002) \text{ mm}$
k_{Bessel}	$(6.138 \pm 0.009) \text{ mm}^{-1}$
w_{Bessel}	$(4.290 \pm 0.118) \text{ mm}$

ically shaped lens (a so-called axicon) is commonly used (see Fig. 2a). Since spin waves propagate in thin films, a corresponding spin-wave axicon is the two-dimensional projection onto the film plane (an isosceles triangle). The incoming Gaussian beam with a diameter d_{beam} passes the optical element centered such that the beam is refracted at the backside in $+y$ and $-y$ direction. The initial beam is divided into two sub-beams with diameter $d_{\text{sub-beam}} = d_{\text{beam}}/2$. Right next to the backside of the optical element both sub-beams interfere. In this area Bessel-Gaussian beams exist in good approximation. The size of the Bessel beam area depends on d_{beam} , the magnonic refractive index of the axicon and its surrounding area, as well as the characteristic angle β_{axicon} . In Figure 3 the obtained results of the micromagnetic simulations are shown. The Bessel beam is non-diffractive²⁸. Moreover, the beam reconstructs its shape after impinging onto an obstacle. Hence, Bessel beams are self-healing²⁹. The beam profile perpendicular to the propagation direction x can be described by a Gaussian distribution and a Bessel function J_i of the first kind (i is an integer). The normalized amplitude of the precessing magnetization's x component m_x can be fitted using the equation

$$\frac{m_x(y)}{m_{x,\text{max}}} = A \cdot J_0\left(k_{\text{Bessel}} \cdot (y - y_0)\right) \cdot e^{-\left(\frac{y - y_0}{w_{\text{Bessel}}}\right)^2} - B. \quad (3)$$

In Fig. 3d beam profiles along cross-sections in the y direction are plotted and compared to the obtained fitting function. The coefficient of determination R^2 is approximately 0.88. Thus, the observed beam is Bessel like. The parameters of the fitting procedure are listed in Table I. Further simulations regarding BVMSW and MSSW modes are provided in the supplementary material (in-plane field $\mu_0 H_{\text{ext}} = 180 \text{ mT}$). The results qualitatively do not differ from Figure 3, although the corresponding dispersion relations are anisotropic.

II. SPIN-WAVE GRIN LENSES

By continuously modifying the materials's parameters, and consequently the magnonic refractive index, the spin-wave propagation can be controlled further. In photonics, such continuous modifications are used in gradient-index optics³⁰. Typical examples are the Fata Morgana, GRIN fibers, and GRIN lenses. A GRIN lens is shown schematically in Fig. 2b. The rays are curved parabolically since the GRIN lens has a

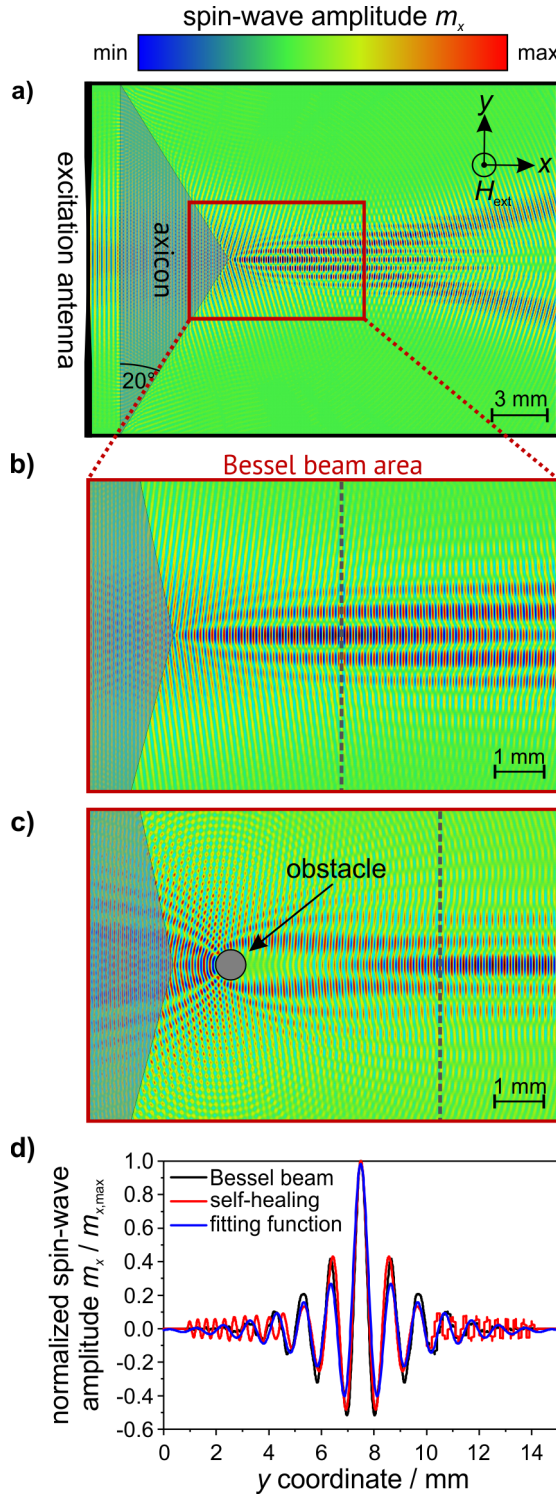


FIG. 3. **a)** Simulation of a spin-wave Bessel beam. **b)** Enlarged Bessel beam area. **c)** Self-healing properties of Bessel beams after hitting a circular hole in the sample with a diameter of $500\mu\text{m}$. **d)** Comparison of the normalized spin-wave amplitudes corresponding to the cross-sections in (b) and (c) (dotted lines). The wavelength in the simulations is $\lambda = 150\mu\text{m}$. For an external magnetic field $\mu_0 H_{\text{ext}} = 300\text{mT}$ this corresponds to a frequency $f \approx 3.78\text{GHz}$. The characteristic angle β_{axicon} is 20° and the $30 \times 15\text{mm}^2$ wide simulation area consists of 2048×2048 cells.

parabolic refractive index profile with the curvature g^{30} :

$$n(r) = n_0 - \Delta n(r) \quad (4)$$

$$= n_0 \cdot \left[1 - \frac{\Delta n(r)}{n_0} \right] \quad (5)$$

$$= n_0 \cdot \left[1 - \frac{g^2}{2} r^2 \right]. \quad (6)$$

Here, r is the radial distance to the optical axis where the refractive index is n_0 . The focal distance f_{GRIN} and working distance s_{GRIN} are given by (L_{GRIN} : thickness of the lens)³⁰:

$$f_{\text{GRIN}} = \frac{1}{n_0 g \sin(g L_{\text{GRIN}})} \approx \frac{1}{n_0 g^2 L_{\text{GRIN}}}, \quad (7)$$

$$s_{\text{GRIN}} = \frac{1}{n_0 g \tan(g L_{\text{GRIN}})} \approx \frac{1}{n_0 g^2 L_{\text{GRIN}}}. \quad (8)$$

For thin lenses f_{GRIN} and s_{GRIN} are equal ($g L_{\text{GRIN}} \ll 1$). In the simulations we use parabolic temperature profiles to create gradient-index lenses:

$$T(r) = T_0 + \Delta T(r) \quad (9)$$

$$= T_0 \cdot \left[1 + \frac{\Delta T(r)}{T_0} \right]. \quad (10)$$

In Figure 4 numerically obtained results for a thin lens with $L_{\text{GRIN}} = 2\text{mm}$ and $\Delta T = 40\text{K}$ are shown. In the focal plane a pronounced increase of the spin-wave amplitude is visible. Comparing Eqs. (5) and (6) it follows:

$$\Delta n \propto g^2 \xrightarrow{(8)} s_{\text{GRIN}} \propto \frac{1}{\Delta n} \xrightarrow{(5)\&(10)} s_{\text{GRIN}} \propto \frac{1}{\Delta T}. \quad (11)$$

The working distance for different temperature or magnonic refractive index differences, respectively, is plotted in Fig. 4b. Additionally, the orientation of the external magnetic field is rotated in-plane to investigate the BVMSW and MSSW modes (see supplementary material, $\mu_0 H_{\text{ext}} = 180\text{mT}$). In case of BVMSWs the parabolic temperature profile has to be inverted, because the dispersion relation $\omega(k)$ is monotonously decreasing with increasing k (in contrast to FVMSWs and MSSWs, see Ref. 21). Equation (11) can be verified by fitting the obtained data in Fig. 4b. The corresponding values of R^2 are larger than 0.97. By comparing the maximal amplitude in the focal plane with the value before passing the lens the amplification factor can be determined. This is shown in Fig. 4c for the investigated modes and the corresponding working distances from Fig. 4b. In the simulations, a maximal amplification factor of 3.8 for the amplitude and of 14.4 for the spin-wave intensity are observed.

III. SPIN-WAVE FOURIER OPTICS

In Fourier optics the propagation of light is described using Fourier analysis, and image modifications can be performed by filtering selected Fourier orders. Just as a lens with curved surfaces a GRIN lens can perform a Fourier transformation^{30,31}. Now we use such GRIN lenses to realize spin-wave Fourier optics (see Fig. 4d for the corresponding setup). The far field in the back focal plane of the first lens

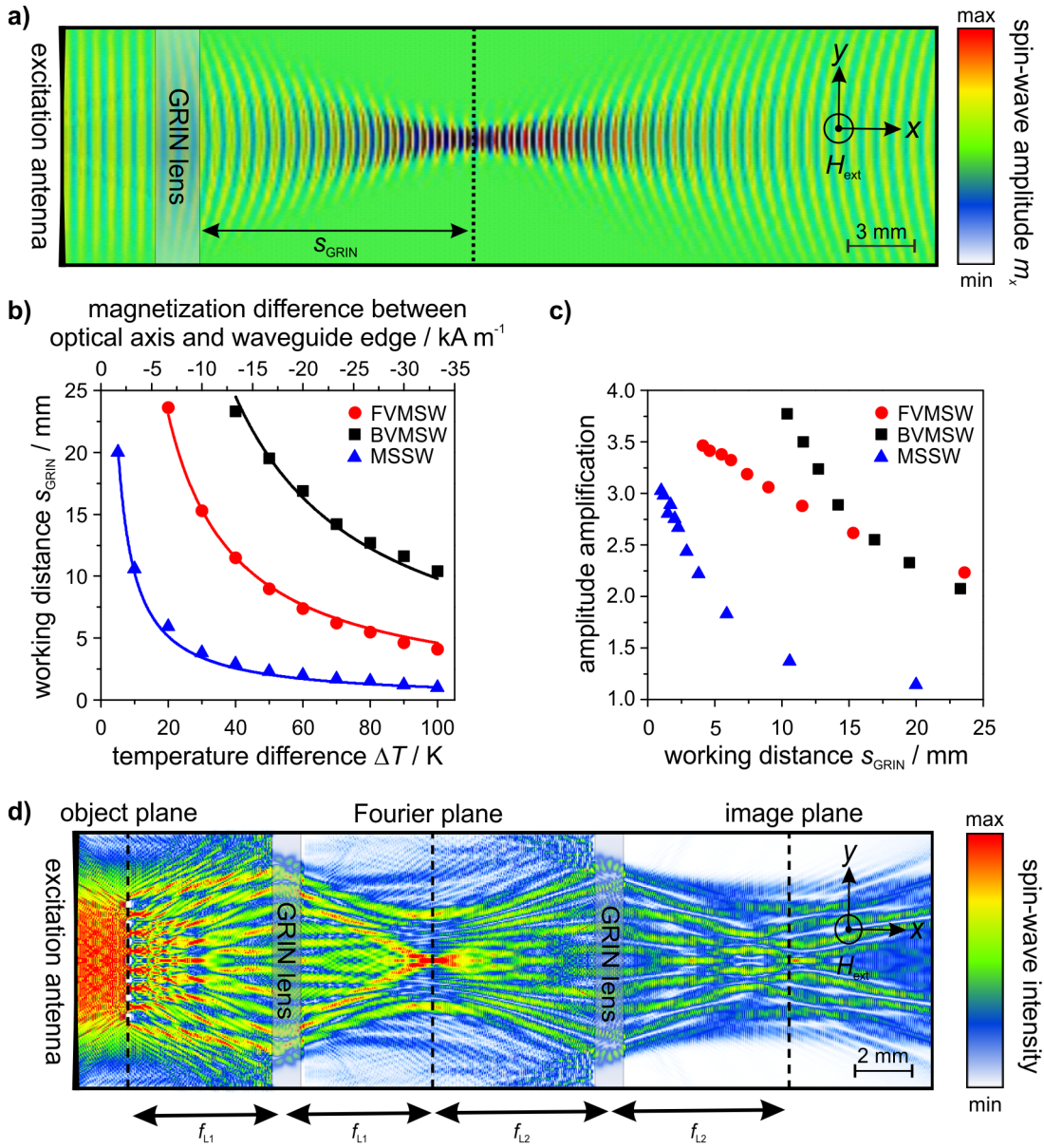


FIG. 4. **a)** Focusing of spin waves using gradient-index lenses. Focusing can be achieved for all spin-wave modes. The external magnetic field is $\mu_0 H_{ext} = 300$ mT for FVMSWs and $\mu_0 H_{ext} = 180$ mT for BVMSWs and MSSWs. **b)** Working distances for different GRIN profiles dependent on the temperature difference between the optical axis and the edge of the lens. **c)** Amplitude amplification for the working distances shown in (b). **d)** GRIN lenses can be used to achieve spin-wave Fourier optics ($f_{L1} \approx f_{L2}$, $L_{GRIN} = 1$ mm, $\Delta T = 50$ K).

is the Fourier transform of the incoming field in the front focal plane ($2f$ setup). If the distance between the lenses equals the sum of the focal lengths, the arrangement is called a $4f$ setup. The object is positioned in the front focal plane of the first lens (object plane). The Fourier plane is in the back focal plane of the first lens or the front focal plane of the second lens, respectively. In the back focal plane of the second lens the image of the object is reconstructed (image plane). The magnification depends on the ratio of the lenses' focal distances f_{L1} and f_{L2} . If $f_{L1} = f_{L2}$ the object is imaged without magnification. In Fig. 4d the object is a grating with 7 lines. Each line measures $100\mu\text{m} \times 200\mu\text{m}$ and the lines

are separated by $600\mu\text{m}$. The corresponding wavevectors resulting from the Fourier transformation are visible as pronounced side maxima in the Fourier plane. The second GRIN lens reconstructs the grating as seven focal points in the image plane. The size of and the separation between the spots is approximately equal to the original grating, demonstrating a spin-wave hardware Fourier transformation.

Conclusions

By changing the magnonic refractive index via e.g. modifying the local saturation magnetization the propagation of different spin-wave modes can be controlled. Despite very

different and strongly anisotropic propagation characteristics, we report on axicons to realize Bessel-Gaussian beams as well as gradient-index lenses to focus spin waves in the FVMSW, BVMSW, and MSSW geometry. Furthermore, the properties of the GRIN lenses can be exploited to perform spin-wave Fourier optics. Since spin waves can be used for information processing³², magnonic gradient-index lenses have the potential to perform a Fourier transform with a single computational element in real-time.

ACKNOWLEDGMENTS

Financial support by the DFG Transregional Collaborative Research Center (SFB/TRR) 173 "Spin + X – Spin in its collective environment" within project B04 is gratefully acknowledged (DFG project number 268565370).

- ¹P. Gruszecki, M. Kasprzak, A. E. Serebryannikov, M. Krawczyk, and W. Smigaj, "Microwave excitation of spin wave beams in thin ferromagnetic films," *Scientific Reports* **6**, 22367 (2016).
- ²J. Stigloher, M. Decker, H. S. Körner, K. Tanabe, T. Moriyama, T. Taniguchi, H. Hata, M. Madami, G. Gubbiotti, K. Kobayashi, T. Ono, and C. H. Back, "Snell's law for spin waves," *Physical Review Letters* **117**, 037204 (2016).
- ³X. Xing and Y. Zhou, "Fiber optics for spin waves," *NPG Asia Materials* **8**, e246 (2016).
- ⁴W. Yu, J. Lan, R. Wu, and J. Xiao, "Magnetic Snell's law and spin-wave fiber with Dzyaloshinskii-Moriya interaction," *Physical Review B* **94**, 140410 (2016).
- ⁵J.-N. Toedt, M. Mundkowsky, D. Heitmann, S. Mendach, and W. Hansen, "Design and construction of a spin-wave lens," *Scientific Reports* **6**, 33169 (2016).
- ⁶O. Dzyapko, I. V. Borisenko, V. E. Demidov, W. Pernice, and S. O. Demokritov, "Reconfigurable heat-induced spin wave lenses," *Applied Physics Letters* **109**, 232407 (2016).
- ⁷J. Gräfe, M. Decker, K. Keskinbora, M. Noske, P. Gawronski, H. Stoll, C. H. Back, E. J. Goering, and G. Schütz, "X-Ray microscopy of spin wave focusing using a fresnel zone plate," *arXiv* **1707.03664** (2017).
- ⁸N. J. Whitehead, S. A. Horsley, T. G. Philbin, and V. V. Kruglyak, "A Luneburg lens for spin waves," *Applied Physics Letters* **113**, 212404 (2018).
- ⁹H. S. Körner, J. Stigloher, and C. H. Back, "Excitation and tailoring of diffractive spin-wave beams in NiFe using nonuniform microwave antennas," *Physical Review B* **96**, 100401 (2017).
- ¹⁰C. S. Davies and V. Kruglyak, "Graded-index magnonics," *Low Temperature Physics* **41**, 10 (2015).
- ¹¹C. S. Davies, A. Francis, A. V. Sadovnikov, S. V. Chertopalov, M. T. Bryan, S. V. Grishin, D. A. Allwood, Y. P. Sharaevskii, S. A. Nikitov, and V. V. Kruglyak, "Towards graded-index magnonics: Steering spin waves in magnonic networks," *Physical Review B - Condensed Matter and Materials Physics* **92**, 020408 (2015).
- ¹²P. Gruszecki and M. Krawczyk, "Spin-wave beam propagation in ferromagnetic thin films with graded refractive index: Mirage effect and prospective applications," *Physical Review B* **97**, 094424 (2018).
- ¹³M. Vogel, R. Aßmann, P. Pirro, A. V. Chumak, B. Hillebrands, and G. von Freymann, "Control of spin-wave propagation using magnetisation gradients," *Scientific Reports* **8**, 11099 (2018).
- ¹⁴M. Krawczyk and D. Grundler, "Review and prospects of magnonic crystals and devices with reprogrammable band structure," *Journal of Physics Condensed Matter* **26**, 123202 (2014).
- ¹⁵M. Vogel, A. V. Chumak, E. H. Waller, T. Langner, V. I. Vasyuchka, B. Hillebrands, and G. von Freymann, "Optically reconfigurable magnetic materials," *Nature Physics* **11**, 487–491 (2015).
- ¹⁶A. V. Chumak and D. January, "Magnonic crystals for data processing," *Journal of Physics D: Applied Physics* **50**, 244001 (2017).
- ¹⁷A. Vansteenkiste, J. Leliaert, M. Dvornik, M. Helsen, F. Garcia-Sanchez, and B. Van Waeyenberge, "The design and verification of MuMax3," *AIP Advances* **4**, 107133 (2014).
- ¹⁸R. W. Damon and H. Van De Vaart, "Propagation of magnetostatic spin waves at microwave frequencies in a normally-magnetized disk," *Journal of Applied Physics* **36**, 3453–3459 (1965).
- ¹⁹A. V. Vashkovsky and E. H. Lock, "Properties of backward electromagnetic waves and negative reflection in ferrite films," *Physics-Uspekhi* **49**, 389 (2006).
- ²⁰E. H. Lock, "The properties of isofrequency dependences and the laws of geometrical optics," *Phys.-Uspekhi* **51**, 375 (2008).
- ²¹A. A. Serga, A. V. Chumak, and B. Hillebrands, "YIG magnonics," *Journal of Physics D: Applied Physics* **43**, 264002 (2010).
- ²²A. V. Chumak, A. A. Serga, B. Hillebrands, and M. P. Kostylev, "Scattering of backward spin waves in a one-dimensional magnonic crystal," *Applied Physics Letters* **93**, 022508 (2008).
- ²³A. V. Chumak, P. Pirro, A. A. Serga, M. P. Kostylev, R. L. Stamps, H. Schultheiss, K. Vogt, S. J. Hermsdoerfer, B. Laegel, P. A. Beck, and B. Hillebrands, "Spin-wave propagation in a microstructured magnonic crystal," *Applied Physics Letters* **95**, 262508 (2009).
- ²⁴A. V. Chumak, T. Neumann, A. A. Serga, B. Hillebrands, and M. P. Kostylev, "A current-controlled, dynamic magnonic crystal," *Journal of Physics D: Applied Physics* **42**, 205005 (2009).
- ²⁵B. Obyr, P. Pirro, T. Brächer, A. V. Chumak, J. Osten, F. Ciubotaru, A. A. Serga, J. Fassbender, and B. Hillebrands, "A micro-structured ion-implanted magnonic crystal," *Applied Physics Letters* **102**, 202403 (2013).
- ²⁶F. Gori, G. Guattari, and C. Padovani, "Bessel-Gauss beams," *Optics Communications* **64**, 491–495 (1987).
- ²⁷J. Arlt, V. Garces-Chavez, W. Sibbett, and K. Dholakia, "Optical micromanipulation using a Bessel light beam," *Optics Communications* **197**, 239–245 (2001).
- ²⁸J. Durnin, J. Miceli, and J. H. Eberly, "Diffraction-free beams," *Physical Review Letters* **58**, 1499–1501 (1987).
- ²⁹V. Garcés-Chávez, D. McGloin, H. Melville, W. Sibbett, and K. Dholakia, "Simultaneous micromanipulation in multiple planes using a self-reconstructing light beam," *Nature* **419**, 145 – 147 (2002).
- ³⁰B. E. A. Saleh and M. C. Teich, *Fundamentals of Photonics*, 2nd ed. (Wiley-VCH, Berlin, 2008).
- ³¹C. Gómez-Reino, E. Acosta, and J. Liñares, "Image and Fourier transform formation by GRIN lenses: pupil effect," *Journal of Modern Optics* **34**, 1501–1510 (1987).
- ³²A. D. Karenowska, A. V. Chumak, A. A. Serga, and B. Hillebrands, "Magnon spintronics," *Handbook of Spintronics* **11**, 1505–1549 (2015).

Spin-Wave Optical Elements: Towards Spin-Wave Fourier Optics
SUPPLEMENTARY MATERIAL

M. Vogel,^{1, a)} B. Hillebrands,¹ and G. von Freymann^{2, 1}

¹⁾*Department of Physics and State Research Center OPTIMAS,
Technische Universität Kaiserslautern (TUK), Erwin-Schrödinger-Str. 56,
67663 Kaiserslautern, Germany*

²⁾*Fraunhofer-Institute for Industrial Mathematics ITWM, Fraunhofer-Platz 1,
67663 Kaiserslautern, Germany*

(Dated: 7 June 2019)

In the main text, axicons to create Bessel-Gaussian beams are discussed in the FMVSW geometry. The external magnetic field is aligned out-of-plane and the thickness of the yttrium iron garnet film is 5 μm . Despite the strong anisotropy in in-plane magnetized films it is also possible to excite such beams in the BVMSW and MSSW geometry. In Figure S1 the corresponding results of micromagnetic simulations are shown. In contrast to FVMSW modes, the phase fronts of the sub-beams are not perpendicular to the propagation direction. Moreover, gradient-index lenses are also possible in in-plane magnetized samples (see Figure S2). The obtained results in Figure S1 and Figure S2 qualitatively do not differ from the FVMSW configuration shown in the main text.

^{a)}Electronic mail: mvogel@physik.uni-kl.de

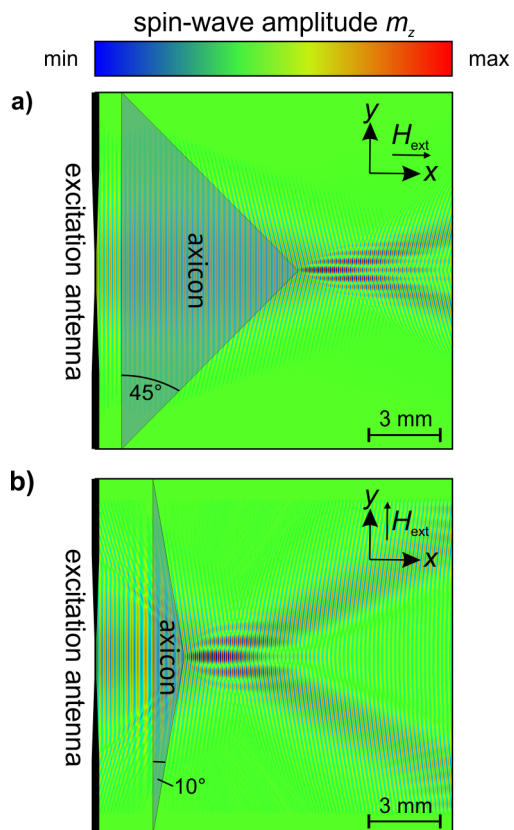


FIG. S1. Axicons to realize Bessel-Gaussian beams for BVMSW (a) and MSSW modes (b). The external magnetic field is aligned in-plane ($\mu_0 H_{\text{ext}} = 180 \text{ mT}$). The background temperature is 298 K. The axicon's temperature differs by 10 K.

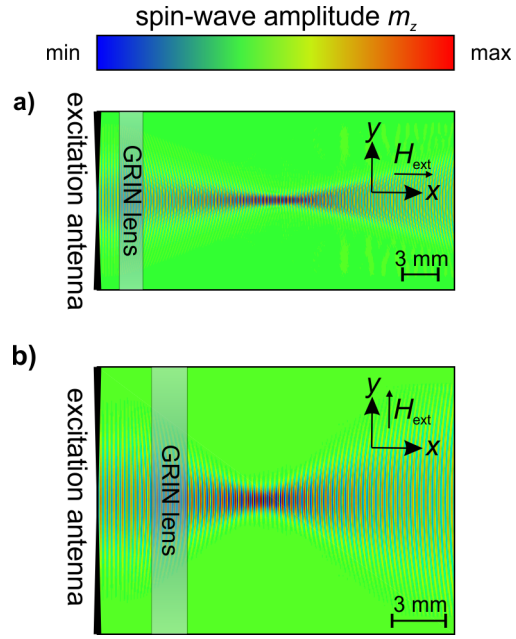


FIG. S2. GRIN lenses to focus BVMSWs **(a)** and MSSWs **(b)**. The external magnetic field is aligned in-plane. The magnitude is $\mu_0 H_{ext} = 180$ mT. The shown lenses are 2 mm wide and the temperature difference ΔT is 40 K in (a) and 10 K in (b)